Solving MAXCUT with Quantum Imaginary Time Evolution

Rizwanul Alam* and George Siopsis†
*Department of Physics and Astronomy,
University of Tennessee at Knoxville
Knoxville, Tennessee 37996-1200 USA*

Rebekah Herrman‡ and James Ostrowski§
*Department of Industrial and Systems Engineering,
University of Tennessee at Knoxville
Knoxville, TN 37996 USA*

Phillip C. Lotshaw¶ and Travis S. Humble**
*Quantum Computing Institute
Oak Ridge National Laboratory
Oak Ridge, TN 37830 USA*
(Dated: December 2021)

We introduce a method to solve the MaxCut problem efficiently based on quantum imaginary time evolution (QITE). We employ a linear *Ansatz* for unitary updates and an initial state involving no entanglement, as well as an imaginary-time-dependent Hamiltonian interpolating between a given graph and a subgraph with two edges excised. We apply the method to thousands of randomly selected graphs with up to fifty vertices. We show that our algorithm exhibits a 93% and above performance converging to the maximum solution of the MaxCut problem for all considered graphs. Our results compare favorably with the performance of classical algorithms, such as the greedy and Goemans-Williamson algorithms. We also discuss the overlap of the final state of the QITE algorithm with the ground state as a performance metric, which is a quantum feature not shared by other classical algorithms.

I.   INTRODUCTION

Since fault-tolerant universal quantum computers have yet to be developed, considerable effort is focused on demonstrating quantum advantage with currently available noisy intermediate-scale quantum (NISQ) devices, including superconducting [1] and photonic [2] quantum computers. An area of practical importance in these explorations is finding approximate solutions to combinatorial optimization problems, such as MaxCut. Finding exact solutions to MaxCut is classically hard, but near optimal solutions can be found classically [3–8]. Quantum algorithms promise a speedup over classical ones. However, it is a challenge to demonstrate their advantage with NISQ devices.

A widely studied quantum algorithm for combinatorial optimization problems which is suitable for NISQ hardware is the quantum approximate optimization algorithm (QAOA) [9]. It has been discussed both theoretically and experimentally [10–23]. Variants of QAOA have also been explored [24–31]. Motivated by adiabatic evolution, QAOA uses a string of unitary evolution operators alternating between two Hamiltonian functions with time parameters that are optimized classically in order to maximize the cost function (equivalently, minimize the energy of the corresponding Hamiltonian). One starts with a state which is not entangled and the desired final state (ground state) need not be entangled. However, the quantum circuit introduces entanglement which is expected to provide quantum advantage in the calculation of the minimum energy eigenvalue. In practice, it is challenging to establish quantum advantage, in the absence of a theoretical argument, because only shallow quantum circuits can be implemented on NISQ hardware without overwhelming quantum errors.

A popular class of classical algorithms applied to MaxCut are the greedy algorithms that rely on greedy vertex labeling or an edge contraction strategy [4–7]. They exhibit a 50% performance for the worst-case graphs. The best worst-case performance is provided by the Goemans-Williamson (classical) algorithm [8] at 88% approximation ratio for MaxCut. It is instructive to look at the performance of QAOA compared to other classical algorithms. It has

---

* ralam4@tennessee.edu
† siopsis@tennessee.edu
‡ rherrma2@tennessee.edu
§ jostrows@tennessee.edu
¶ lotshawpc@ornl.gov
** humblets@ornl.gov

been shown that *quantum-inspired optimization* methods, such as the local tensor method, outperform single-step QAOA on triangle free graphs [32, 33]. There are other studies [34] showing that local classical MaxCut algorithms outperform $p = 2$ QAOA on regular graphs of girth ≥ 5. In a study of more generalized problems, e.g., approximately solving instances of Max k XOR, calculations have been performed to obtain numerical upper and lower bounds on local classical and quantum algorithms for triangle-free instances [35].

Here we discuss a different method to solve combinatorial optimization problems, focusing on MaxCut, based on quantum imaginary time evolution (QITE). The QITE algorithm has been widely used to find the ground-state energy of many-particle systems [36, 37]. Since evolution in imaginary time effectively cools the system down to zero temperature [38], the ground state can be prepared with QITE exactly without any variational optimization. However, in practice, due to limited computational resources, approximations must be made calling for an approach involving variational calculus. An approach to QITE for the computation of the energy spectrum of a given Hamiltonian was outlined in [39]. It had the advantage compared to a variational quantum eigensolver (VQE) of not using ancilla qubits. The method was applied to the quantum computation of chemical energy levels on NISQ hardware [40–43], and the simulation of open quantum systems [44]. The impact of noise on QITE in NISQ hardware was addressed in [45] using error mitigation and randomized compiling. Error mitigation was also addressed with a different method based on deep reinforcement learning [46]. A reduction of the depth of quantum circuits for QITE using a nonlocal approximation was discussed in [47]. Real and imaginary time evolution with compressed quantum circuits on NISQ hardware were performed in [48].

For the MaxCut problem, QITE can be formulated to introduce entanglement similar to QAOA. Moreover, entanglement may also be present in the initial state, which is arbitrary when the QAOA evolution operators are adjusted appropriately [49], as long as it has finite overlap with the ground state. Following [39], we implement QITE in a string of small steps each involving a unitary update. Similar to QAOA, the unitary operator in each QITE step involves variational parameters, but unlike QAOA, these parameters are fixed by algebraic equations. We chose an initial state and unitary updates that contained no entanglement. This gives a classical baseline for QITE performance, which can be compared to entangling *Ansätze* in future work to assess the role of entanglement. We applied the QITE method with these choices to the MaxCut problem on graphs with up to fifty vertices. Remarkably, within eleven QITE steps on average, we obtained solutions which were on average at 89% or better of the optimal solution. As the number of vertices increased from eight to fifty, the performance of the algorithm remained high dropping from 99% to 89%. Regarding efficiency, each QITE step involves the solution of algebraic equations with number of manipulations $O(|V|^2)$. The number of QITE steps needed also appears to depend polynomially on the number of vertices $|V|$, although further analysis of higher-order graphs is needed to better determine this dependence. These results indicate that our linear QITE method is efficient and quantum advantage due to entanglement is likely to be found only at larger graphs requiring deep quantum circuits which cannot currently be handled by NISQ hardware.

Moreover, a slight modification of our method which also introduced no entanglement, led to above 93% performance for all graphs with up to fifty vertices that we studied. The modification involved an imaginary-time-dependent Hamiltonian interpolating between the given graph and a subgraph with two edges excised within a few QITE steps. Identifying the two edges resulting in evolution leading to the ground state introduces a polynomial overhead in the algorithm. Further work with larger graphs is required to identify the point of failure of this modified QITE method.

Our discussion is organized as follows. In Section II, we introduce the QITE method with our linear *Ansatz* that involves no entanglement applied to the MaxCut problem. In Section III, we present our results on thousands of randomly selected graphs with up to fifty vertices showing that our method always works on all the graphs we studied. Finally in Section IV, we offer concluding remarks.

II.   QITE FOR MAXCUT

In this Section, we introduce our QITE method applied to the MaxCut problem. We employ a linear *Ansatz* for unitary updates which introduces no entanglement. Numerical results are presented in the next Section, where we apply the method to thousands of randomly selected graphs with up to fifty vertices. Remarkably, despite performing approximations at each QITE step, the method always converged to the optimal solution of the MaxCut problem for all the graphs we examined.

Given a graph $G = (V, E)$ consisting of a set of vertices V and edges $E \subseteq V \times V$ joining the vertices in V, the MaxCut problem on G is the combinatorial optimization problem of partitioning V into two disjoint sets such that the number of edges with endpoints in each set, C, is maximized ($C = C_{\max}$). It can be formulated as a Hamiltonian ground-state problem by associating a qubit with every vertex in V and defining the Hamiltonian

$$H = \sum_{(ij) \in E} Z_i Z_j \tag{1}$$

where Z_i is a Pauli Z-matrix acting on the qubit at the ith vertex. Here, the eigenstates of H are computational basis states $|z\rangle = \bigotimes_{j=1}^{|V|}|z_j\rangle$, where $z_j \in \{0,1\}$, and $|z_j\rangle$ is the state of the qubit at the jth vertex. The solution C_{max} to the MaxCut problem is related to the ground-state energy E_0 of H by

$$C_{max} = \frac{|E| - E_0}{2} \tag{2}$$

All eigenvalues of the Hamiltonian correspond to solutions of the MaxCut problem which are not necessarily optimal,

$$C_k = \frac{|E| - E_k}{2} \quad , \quad k = 0, 1, \ldots, 2^{|V|} - 1 \tag{3}$$

Evidently, $C_k/C_{max} \le 1$.

To find the ground-state energy, the QITE algorithm relies on the fact that any state with non-vanishing overlap with the ground state eventually reduces to the ground state if it is evolved in imaginary time. In other words, the state

$$|\Omega\rangle = \lim_{\beta \to \infty} |\Psi(\beta)\rangle \ , \quad |\Psi(\tau)\rangle \equiv \frac{e^{-\tau H}|\Psi\rangle}{\|e^{-\tau H}|\Psi\rangle\|} \tag{4}$$

is the ground state for any state $|\Psi\rangle$, as long as $\langle\Omega|\Psi\rangle /= 0$,

$$H|\Omega\rangle = E_0|\Omega\rangle \tag{5}$$

The imaginary time parameter β can also be thought of as the inverse temperature ($\beta = \frac{1}{k_B T}$, where T is temperature and k_B is the Boltzmann constant), in which case Eq. (4) states that the system settles to the ground state at zero temperature.

To implement (4), we perform evolution in small imaginary time intervals τ. Starting with $|\Psi[0]\rangle$, suppose that after $s-1$ steps we arrive at the state $|\Psi[s-1]\rangle$. At the next (sth) step, we wish to construct the state

$$|\Psi'(\tau)\rangle = \frac{e^{-\tau H}|\Psi[s-1]\rangle}{\|e^{-\tau H}|\Psi[s-1]\rangle\|} \tag{6}$$

The state $|\Psi'(\tau)\rangle$ has lower energy than $|\Psi[s-1]\rangle$ for sufficiently small τ. To see this, calculate the derivative of the average energy with respect to τ. We obtain

$$\frac{d}{d\tau} \langle\Psi'(\tau)|H|\Psi'(\tau)\rangle \Big|_{\tau=0} = -2(\Delta E[s-1])^2 \tag{7}$$

where $\Delta E[s-1]$ is the uncertainty in energy ($\Delta E = \sqrt{\langle H^2\rangle - \langle H\rangle^2}$ in the state $|\Psi[s-1]\rangle$. It follows that the derivative is negative and the energy is a decreasing function at $\tau = 0$. This step does not decrease the energy if the uncertainty vanishes, $\Delta E[s-1] = 0$. This is the case when the state $|\Psi[s-1]\rangle$ is an eigenstate of the Hamiltonian. If the eigenstate is the ground state, then no further steps are needed. However, it can be an excited state, and then the algorithm fails to reach the ground state. It would be desirable to understand how the structure of graphs influences the final state and how one can overcome convergence to an excited energy state.

As we will see, in order to avoid reaching an excited state, it is advantageous to interpolate between a Hamiltonian that corresponds to a subgraph of G and H. We therefore define

$$H[s] \equiv \sum_{(ij)\in E} h_{ij}[s]Z_iZ_j \tag{8}$$

where all $h_{ij}[s] \to 1$ for large enough s (say, $h_{ij}[s] = 1$, for $s \ge s_0$), so that $H[s] \to H$. To select a given subgraph of G as starting point, the coefficients that do not correspond to an edge in the subgraph are set to vanish initially as described further in the next Section.

The state $|\Psi'(\tau)\rangle$ is approximated by a unitary acting on $|\Psi[s-1]\rangle$, $e^{-i\tau A[s]}$, where $A[s]$ is a Hermitian operator. Then after s steps, we arrive at the state

$$|\Psi[s]\rangle = e^{-i\tau A[s]}|\Psi[s-1]\rangle \tag{9}$$

This is done by minimizing the distance $\delta = \||\Psi[s]\rangle - |\Psi'(\tau)\rangle\|$ between the approximately evolved state (9) and the desired state, (6), where we used the definition $\||\Phi\rangle\| = \sqrt{\langle\Phi|\Phi\rangle}$ for the norm of a state $|\Phi\rangle$. At first order in the

small imaginary time parameter τ, minimizing δ leads to a linear system of algebraic equations that can be used to determine the free parameters in $A[s]$. We may expand $A[s] = A_1[s] + A_2[s] + \ldots$, where $A_k[s]$ is a linear combination of products of k Pauli matrices ($k = 1, 2, \ldots$). Including higher values of k brings the distance δ closer to zero at the expense of increasing the complexity of the calculation. To perform a systematic study, we start by including terms with $k = 1$ only, and leave the inclusion of higher-order terms in $A[s]$ to future work.

Thus, to determine this unitary update, we adopt the *linear Ansatz*

$$A[s] = \sum_{j \in V} a_j[s] Y_j \tag{10}$$

where Y_j is the Y-Pauli matrix acting on the qubit at the jth vertex. It is straightforward to see [39] that the distance δ is minimized for coefficients $a_j[s]$ obeying the linear system of equations

$$\boldsymbol{S} \cdot \boldsymbol{a} = \boldsymbol{b}, \quad S_{ij}[s] = \langle Y_i Y_j \rangle, \quad b_j[s] = -\frac{i}{2}\langle [H, Y_j] \rangle \tag{11}$$

where all expectation values are evaluated with respect to the state $|\Psi[s-1]\rangle$ obtained in the previous step. Notice that the commutator in $\boldsymbol{b}$ can be written as

$$[H, Y_j] = -2iH_j H_{G_j} H_j \tag{12}$$

where we used $HZH = X$ with H_j being the Hadamard matrix H acting on the qubit at the jth vertex, and G_j the subgraph of G consisting of the vertex j and its adjacent vertices in G with Hamiltonian

$$H_{G_j} = \sum_{(ij) \in E(G_j)} h_{ij} Z_i Z_j \tag{13}$$

Since H_{G_j} is diagonal in the computational basis, $b_j[s]$ can be computed by engineering the state $H_j|\Psi[s-1]\rangle$, measuring each qubit, and using

$$b_j[s] = -\langle \Psi[s-1] | H_j H_{G_j} H_j | \Psi[s-1] \rangle \tag{14}$$

Similarly, the matrix elements of $\boldsymbol{S}$ can be expressed in terms of expectation values involving the two-qubit matrix $Z_i Z_j$ which is diagonal in the computational basis,

$$S_{ij}[s] = \langle \Psi[s-1] | e^{i\frac{\pi}{4}(X_i + X_j)} Z_i Z_j e^{-i\frac{\pi}{4}(X_i + X_j)} | \Psi[s-1] \rangle \tag{15}$$

where we used $e^{i\frac{\pi}{4}X} Z e^{-i\frac{\pi}{4}X} = Y$, and can be obtained by engineering the state $e^{-i\frac{\pi}{4}(X_i + X_j)}|\Psi[s-1]\rangle$ and measuring all qubits.

It should be noted that the unitary updates (9) with the linear *Ansatz* (10) do not introduce entanglement. If one starts with a separable initial state, the state at each step in the QITE algorithm will be separable. A further simplification occurs if the initial state is chosen to be the tensor product of eigenstates of X and Z,

$$|\Psi[0]\rangle = \bigotimes_{j=1}^{|V|} |s_j\rangle \tag{16}$$

where $|s_j\rangle \in \{|0\rangle, |1\rangle, |+\rangle, |-\rangle\}$, and $|\pm\rangle = \frac{1}{\sqrt{2}}(|0\rangle \pm |1\rangle)$. In this case, the matrix $\boldsymbol{S}$ is the identity, because $\langle s_j | Y_j | s_j \rangle = 0$. It follows that $\boldsymbol{a} = \boldsymbol{b}$. It is easy to see that single-qubit states should not all be eigenstates of X, because they yield $\boldsymbol{a} = \boldsymbol{0}$, due to $\langle \pm | Z | \pm \rangle = 0$ in (11). Let us change the state of the qubit at position j to $|0\rangle$. Then we obtain non-vanishing coefficients $a_i[s]$ for the qubits that are adjacent to j, i.e., $a_i[s] \neq 0$ for $(ij) \in E$. At the next step in the QITE algorithm, we obtain non-vanishing coefficients for all qubits at distance up to 2 from the one at position j. For a connected graph, it takes less than $|V|$ steps to obtain non-vanishing coefficients for all qubits.

After s steps in the QITE algorithm, we arrive at the state

$$|\Psi[s]\rangle = e^{-i\tau A[s]} |\Psi[0]\rangle, \quad A[s] = \sum_{s'=1}^{s} A[s'] \tag{17}$$

In our calculations, we chose an initial state in which all qubits were set to $|+\rangle$, except one which was set to $|0\rangle$. We chose the latter qubit to be at one of the highest-degree vertices. This is an arbitrary choice, but appears to be more efficient in some cases. Thus,

$$|\Psi[0]\rangle = H_j |\Psi_0\rangle, \quad |\Psi_0\rangle = |+\rangle^{\otimes |V|} \tag{18}$$

where H_j is the Hadamard matrix at the position of the chosen qubit, and $|\Psi_0\rangle$ is the standard initial choice in QAOA.

At the sth QITE step, we used the unitary update $e^{-i\tau A[s]}$ and optimized the choice of the small imaginary-time parameter τ by minimizing the average energy $\langle H \rangle$ of the state at the sth step. Note that this involves computing all the intermediary states $|\Psi[s']\rangle$ to evaluate the coefficients $a_j[s']$ in (11), for all $s' < s$.

Regarding efficiency, we note that at each QITE step, we need to solve a system of algebraic equations which requires a number of manipulations which is polynomial in the number of vertices $|V|$ of the given graph. Moreover, as we show in Section III, with just 5 QITE steps it is possible to achieve more than 88% of $C/C_{\max}$. With an average of 10 steps, it goes over 93% for $|V| \leq 50$. Performance can be further improved with more steps and by making the Hamiltonian imaginary-time dependent, as discussed in Section III. On the metric of ground-state overlap, we find that 75% or more graphs in the random sample we considered have non-zero overlap with the ground state. This can also be further improved by increasing the number of steps and a thorough study of imaginary-time dependent Hamiltonian. Although more work is needed with higher-order graphs, these results point to an efficient method of solving the MaxCut problem for graphs with up to at least 50 vertices, that does not require unitary updates with a higher-order *Ansatz*.
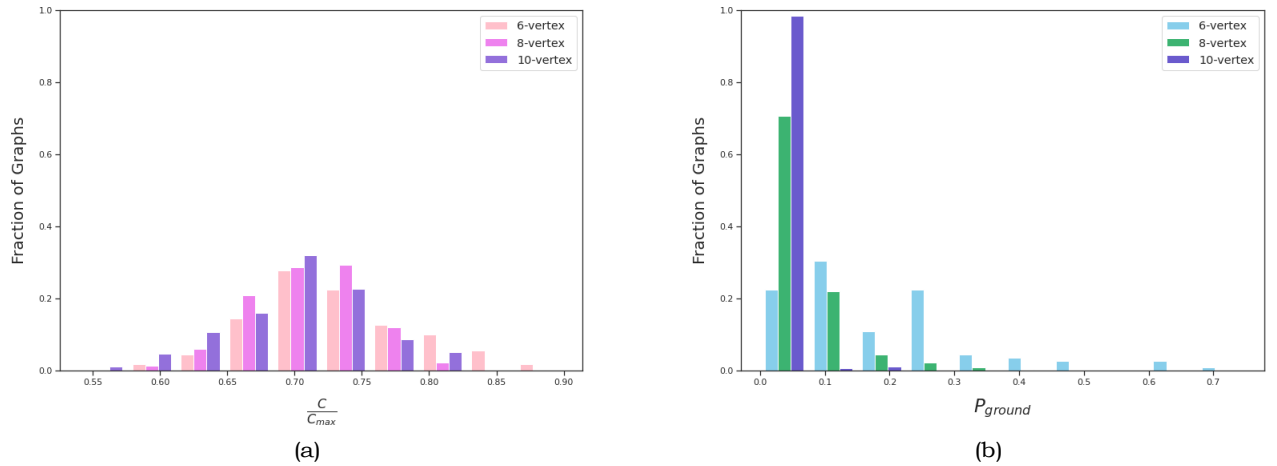
III. RESULTS

FIG. 1. Histograms of (a) $C/C_{\max}$ and (b) probability of overlap with ground state P_{ground} after $s = 1$ QITE step with fixed Hamiltonian for all connected six- and eight-vertex graphs, and 200 randomly chosen connected ten-vertex graphs. The average values of $C/C_{\max}$ are 0.73, 0.71, and 0.70, for six-, eight-, and ten-vertex graphs, respectively. The corresponding average values of P_{ground} are 0.2, 0.06, and 0.02.

In this Section, we present our results of applying the QITE algorithm with a linear *Ansatz* to graphs with up to fifty vertices.

We applied our algorithm to all graphs with up to eight vertices since there is a computationally manageable number of such graphs (e.g., there are only 11,117 distinct graphs with eight vertices). We employed two metrics to assess the performance of our algorithm. One is the average value of $C/C_{\max}$ which is called the approximation ratio and is a metric shared by both classical and quantum algorithms. The other is the overlap of the final state with the ground state that leads to the probability P_{ground} that a measurement yields the ground state of the Hamiltonian, and therefore the optimal solution $C_{\max}$ to the MaxCut problem.

Figure 1 shows the results of applying one step of the QITE algorithm with a linear *Ansatz* to all connected six- and eight-vertex graphs, and 200 randomly selected ten-vertex graphs. We used a fixed Hamiltonian, setting all coefficients $h_{ij} = 1$ in Eq. (13). We obtained average values of $C/C_{\max}$ 73%, 71%, and 70%, for six-, eight-, and ten-vertex graphs, respectively. For the probability P_{ground} we obtained corresponding average values of 20%, 6%, and 2%. In terms of the latter metric, the performance drops significantly as the number of vertices in the graphs increases.
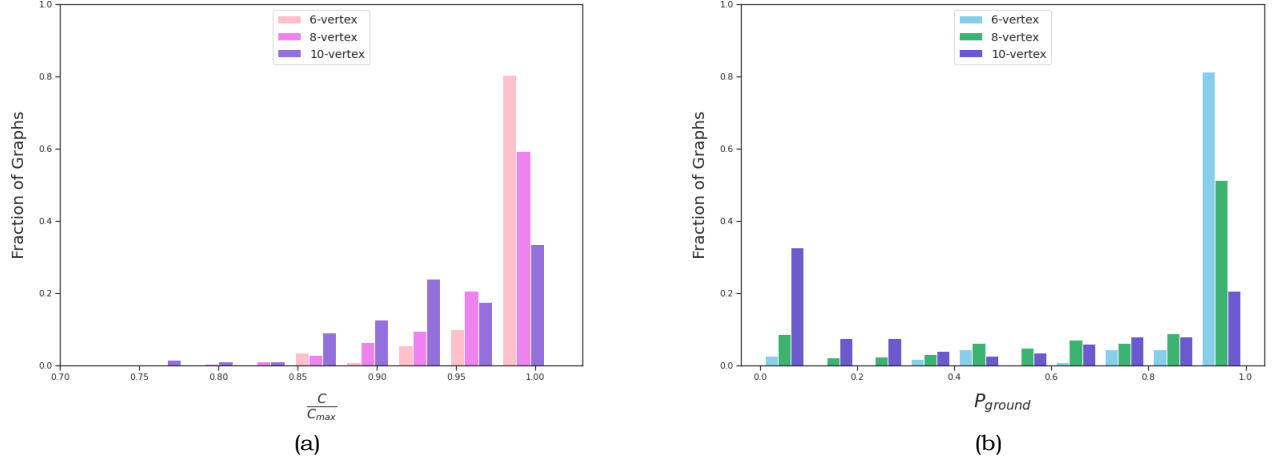
FIG. 2. Histograms of (a) $C/C_{\max}$ and (b) probability of overlap with ground state P_{ground} after $s = 4$ QITE steps with fixed Hamiltonian for all connected six- and eight-vertex graphs, and 200 randomly chosen ten-vertex graphs. The average values of $C/C_{\max}$ are 0.99, 0.96, and 0.95, for six-, eight-, and ten-vertex graphs, respectively. The corresponding average values of P_{ground} are 0.91, 0.66, and 0.48.

The performance of our algorithm improves dramatically after $s = 4$ QITE steps, as shown in Figure 2. We obtained average values of $C/C_{\max}$ 99%, 97%, and 94%, and probabilities P_{ground} 91%, 74%, and 45%, for six-, eight-, and ten-vertex graphs, respectively. These results continued to improve with more QITE steps, although there is not much room for further improvement of $C/C_{\max}$, as the values are very close to 100%. At the tenth QITE step, the algorithm yields a final state which is very close to the one it converges to eventually. Figure 3 shows that at $s = 10$ QITE steps, the average values of $C/C_{\max}$ are 99%, 99%, and 98%, and average probabilities P_{ground} are 94%, 94%, and 74%, for six-, eight-, and ten-vertex graphs, respectively. A comparison of average $C/C_{\max}$ and P_{ground} values at $s = 1, 4, 10$ QITE steps is summarized in Figure 4. As expected, there is a degradation of performance as the number of vertices increases, but this appears to be a small effect. In terms of the probability metric P_{ground}, we obtained a polarized histogram with a large accumulation at 100% and a smaller one at 0%. The 10%, 20%, 25% of six-, eight-, ten-vertex graphs, respectively, with close to zero overlap with the ground state after $s = 4$ QITE steps (Figure 2(b)) remained there in subsequent QITE steps (see Figure 3(b)). This is because the algorithm converges to an eigenstate of the Hamiltonian, which effectively terminates the algorithm as eigenstates are orthogonal to the ground state and do not update in the imaginary-time evolution (6). For the majority of graphs, this is the ground state corresponding to the optimal solution $C_{\max}$. However, for a small percentage of graphs, the algorithm converges to an excited energy level. This still yields a large value of the metric $C/C_{\max}$, but the final state the algorithm converges to is an eigenstate of the Hamiltonian and therefore orthogonal to the ground state, which yields a value of the metric $P_{\text{ground}} = 0$.

One may try to gain insight into the cases in which QITE under-performs by analyzing the graphs for which the probability P_{ground} is small. For example, after $s = 4$ QITE steps, about 20% of the eight-vertex graphs have probability P_{ground} below 0.2%. It is interesting to compare this result with the performance of classical algorithms, such as greedy algorithms [4–7] or the Goemans-Williamson algorithm [8]. Classical (non-probabilistic) algorithms give $P_{\text{ground}} = 0$ on graphs for which they fail to reach $C_{\max}$. A comparison of the sets of graphs on which the greedy algorithms and the linear QITE algorithm, respectively, under-perform may elucidate the cause of such performance. Unfortunately, such a comparison does not appear to yield insights. For example, focusing on the Eulerian graphs, of which there are 184 out of a total of 11,117 connected eight-vertex graphs, after ten QITE steps, our method succeeded equally well on the Eulerian as well non-Eulerian graphs, unlike greedy algorithms. Further simulations are needed to determine how the structure of a graph impacts the performance of our linear QITE algorithm.

Next, we discuss examples of graphs with the worst performance of our linear QITE algorithm in terms of the $C/C_{\max}$ metric with the probability metric $P_{\text{ground}} = 0$. It should be pointed out that even in these worst-performing cases, we obtain values of the $C/C_{\max}$ metric above 70%. As we will show, it is possible to attain above 93% performance in all cases in terms of both metrics $C/C_{\max}$ and P_{ground} with a slight modification of our algorithm.

An example of worst-performing six-vertex graph is shown in Figure 5(a). After applying $s = 10$ QITE steps, we obtain $C = 6$ whereas $C_{\max} = 7$. Thus, QITE has a performance of 86% in terms of the $C/C_{\max}$ metric. Moreover, the probability of overlap with the ground state is zero, and further application of our linear QITE algorithm will
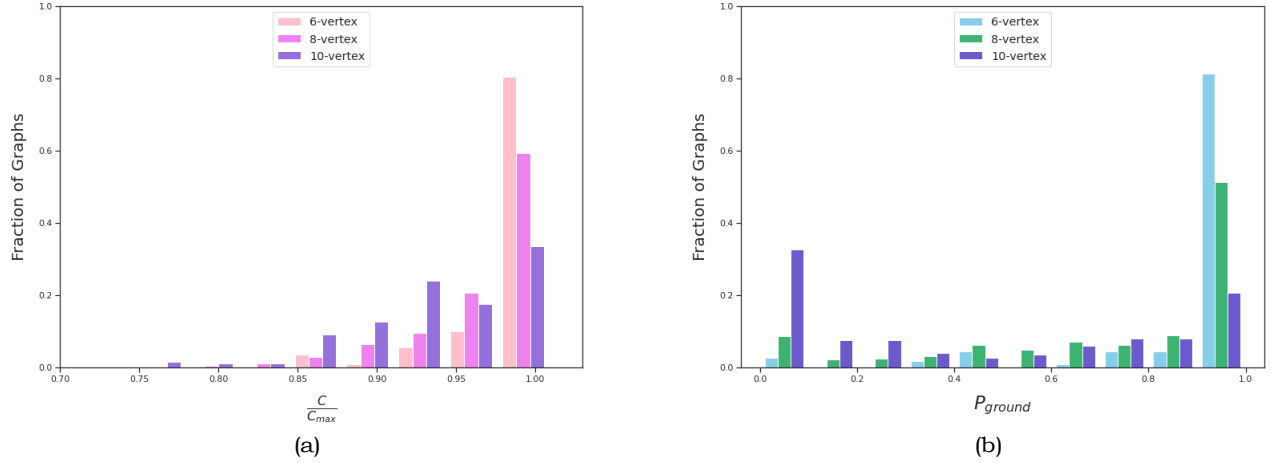
FIG. 3. Histograms of (a) $C/C_{\max}$ and (b) probability of overlap with ground state P_{ground} after $s = 10$ QITE steps with fixed Hamiltonian for all possible connected six- and eight-vertex graphs, and 200 randomly chosen ten-vertex graphs. The average values of $C/C_{\max}$ are 0.99, 0.98, and 0.97, for six-, eight-, and ten-vertex graphs, respectively. The corresponding average values of P_{ground} are 0.94, 0.84, and 0.71.
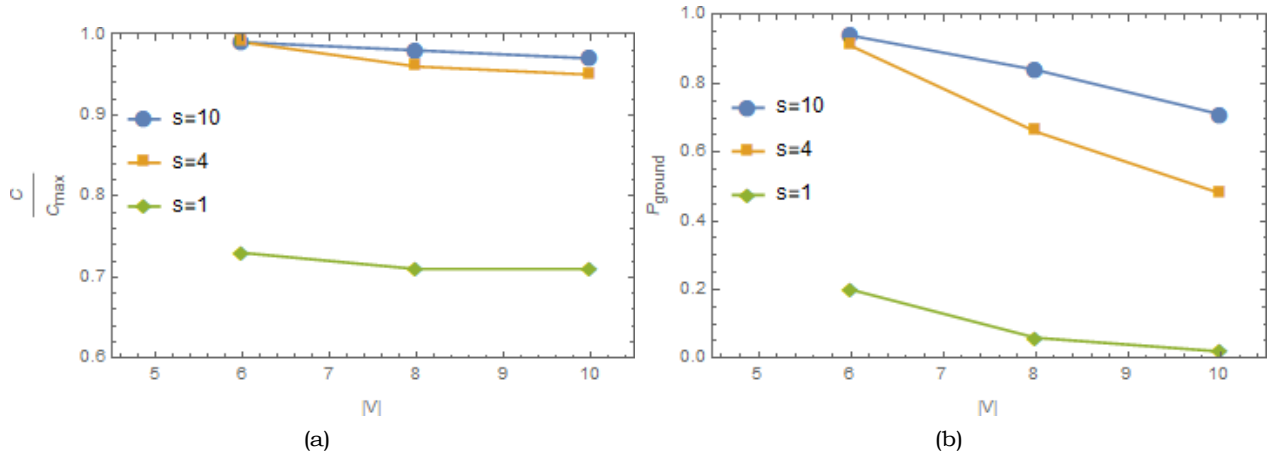

FIG. 4. Average (a) $C/C_{\max}$ and (b) P_{ground} for six-, eight-, and ten-vertex graphs after $s = 1, 4, 10$ QITE steps.

not improve its performance. This is because the algorithm converges to the state $|0\rangle^{\otimes 3} \otimes (\cos\theta|0\rangle - \sin\theta|1\rangle)^{\otimes 2} \otimes |0\rangle$, where $\tan\theta = \frac{1}{9}$, which is in the span of the first-excited states with energy $E_1 = -3$, whereas the ground state $|110001\rangle$ has energy $E_1 = -5$.

An example of worst-performing eight-vertex graph is shown in Figure 5(b). After applying $s = 10$ QITE steps, we obtained $C = 7$, whereas $C_{\max} = 10$. Thus, $C/C_{\max} = 0.7$. Once again, the probability of overlap with the ground state is zero, because our algorithm converges to the third excited state with energy $E_3 = -3$. More QITE steps will not move the state away from this eigenstate and towards the ground state of H (of eigenvalue $E_0 = -9$). Ground states are $|\mathbf{30}\rangle = |00011110\rangle$ and $|\mathbf{225}\rangle = |11100001\rangle$ (written in binary notation), where the latter is obtained from the former by flipping all qubits. The state we end up with after $s = 10$ QITE steps is $|0001\rangle \otimes (\cos\theta|0\rangle + \sin\theta|1\rangle)^{\otimes 2} \otimes |11\rangle$, where $\tan\theta = 0.5$. It is a linear combination of the states $|\mathbf{19}\rangle, |\mathbf{23}\rangle, |\mathbf{27}\rangle, |\mathbf{31}\rangle$, all of which are eigenstates of the Hamiltonian with corresponding eigenvalue $E_3 = -3$.

An example of worst-performing ten-vertex graph is shown in Figure 5(c). We obtained convergence to $C = 16$, whereas $C_{\max} = 17$. Thus, $C/C_{\max} = 0.94$ whereas the probability of overlap with the ground state is zero, because our algorithm converged to the first excited state $|\mathbf{188}\rangle = |0010111100\rangle$ with energy $E_1 = -11$ which is orthogonal to the ground states $|\mathbf{339}\rangle = |0101010011\rangle$ and $|\mathbf{684}\rangle = |1010101100\rangle$ with energy $E_0 = -13$.

Interestingly, the performance can be improved further by considering an imaginary-time-dependent (ITD) Hamil-
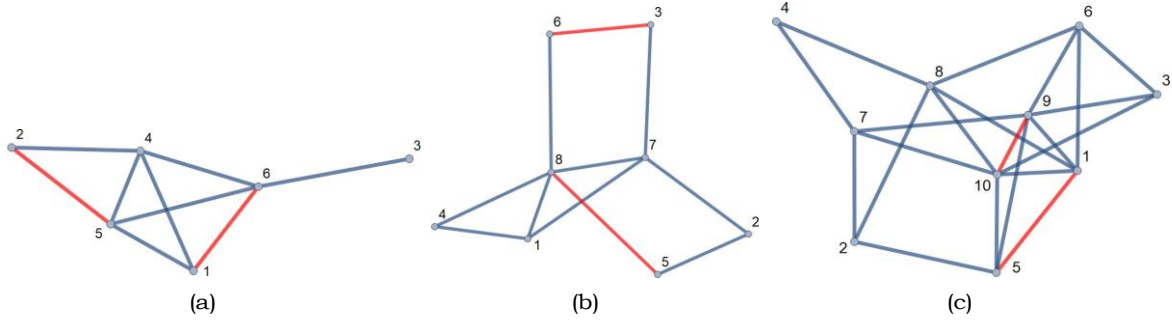
FIG. 5. Example graphs on which our linear QITE algorithm under-performs: (a) 6-vertex, (b) 8-vertex, and (c) 10-vertex graphs.
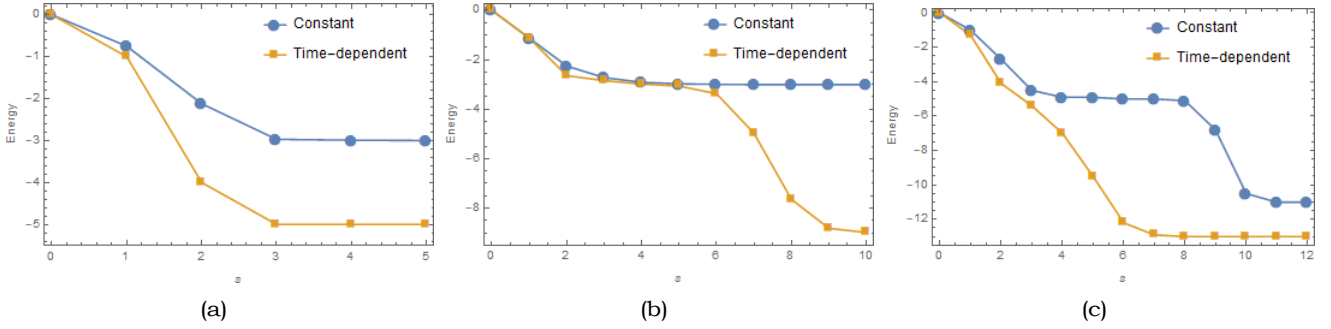

FIG. 6. Convergence of our linear QITE algorithm for Hamiltonian with constant coefficients to energy levels −3, −3, −11, compared with imaginary-time-dependent Hamiltonian to ground state energy −5, −9, −13, for the six-, eight-, and ten-vertex graph, respectively, in Figure 5.

tonian (Eq. (8)). To this end, we start the time evolution along a different path in terms of updates with respect to the imaginary-time-dependent $H_{G_j}[s]$, thereby evading the standard path which results in convergence to an excited state. Let H_G be the Hamiltonian corresponding to the graph $G = (V, E)$ of interest, and $H_{G'}$ the Hamiltonian for a subgraph $G' = (V', E')$ of G. Initially, we excise G' and gradually turn it on to form the graph G we are interested in. This leads us to consider the Hamiltonian with ITD edges,

$$H[s] = H_G - f(s)H_{G'} \qquad (19)$$

where $f(s)$ interpolates between 1 for $s = 1$ and 0 for large s ($s \geq s_0$ for a given s_0), interpolating between the graph G and its subgraph in which G' has been excised. In terms of the weights h_{ij} in Eq. (8), we have constant weights $h_{ij} = 1$, for edges not in G' ($(ij) \notin E'$), and $h_{ij} = 1 - f(s)$, for $(ij) \in E'$.

For the six-vertex graph in Figure 5(a), by excising two edges ($E' = \{(16), (25)\}$), and switching them back on in three QITE steps ($f(1) = 1$, $f(2) = 0.5$, and $f(s) = 0$ for $s > 2$), we obtained convergence to the ground state, and therefore performance of 100% in both metrics C/C_{max} and P_{ground}. A comparison between the Hamiltonian with constant coefficients and the interpolating Hamiltonian is shown in Figure 6(a). For the subgraph G' to be excised, we found 11 different possibilities consisting of pairs of edges out of $\binom{9}{2} = 36$ possible combinations for which our algorithm successfully converged to the ground-state.

Similarly, for the eight-vertex graph in Figure 5(b), we obtained convergence to the ground state by excising G' consisting of the pair of edges $E' = \{(36), (58)\}$. It turned out that out of all $\binom{11}{2} = 55$ combinations, 17 yielded convergence to the ground state. For the ten-vertex graph in Figure 5(c), convergence to the ground state was obtained for 40 different G' subgraphs consisting of pairs of edges out of $\binom{18}{2} = 153$ possible combinations. A comparison between the Hamiltonian with constant coefficients and the interpolating Hamiltonian is shown in Figures 6(b) and 6(c) for the eight- and ten-vertex graphs, respectively.

Motivated by the success of the modified linear QITE algorithm with ITD Hamiltonian on the worst-performing graphs in Figure 5, we applied the strategy of gradually switching on a pair of edges to the remaining graphs on which our linear QITE algorithm under-performed, i.e, it was not 100% successful and did not converge to the ground state that would yield the optimal MaxCut solution. Out of all 112 connected six-vertex graphs, our linear QITE algorithm

using a Hamiltonian with constant weights led to convergence to the ground state for 101 of them. For the remaining 11 graphs, we obtained convergence to the first excited state. Using an ITD Hamiltonian with an appropriate choice of a pair of ITD weighted edges, we obtained convergence to the ground state for all remaining 11 graphs.
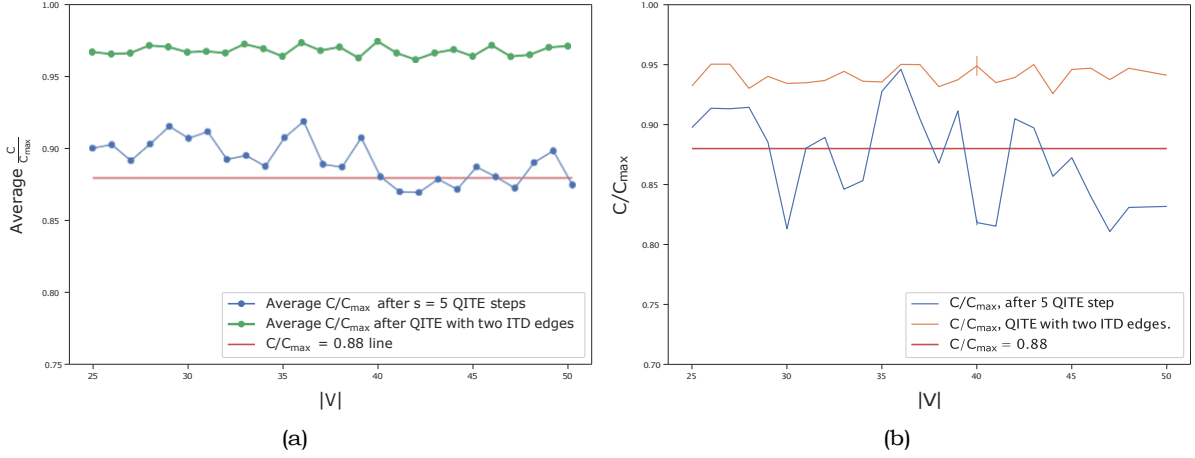

FIG. 7. (a) Average C/C_{max} $vs.$ number of vertices. The blue line is the result of applying s = 5 QITE steps, and the green line is the result of applying QITE with two ITD edges. (b) C/C_{max} $vs.$ number of vertices for the worst performing graphs computed with five-step linear QITE (blue line) and modified QITE with ITD edges (orange line). For reference to classical algorithms, the 88% worst-performance level of the Goemans-Williamson algorithm is indicated with a red line.
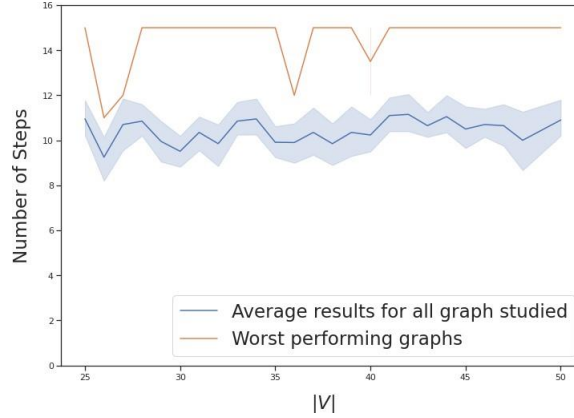

FIG. 8. Average number of steps to reach C/C_{max} of at least 93% $vs.$ number of vertices.

Similar results were obtained for eight-vertex graphs. Our linear QITE algorithm with constant weights led to convergence to the ground state for 8,995 graphs out of all 11,117 connected eight-vertex graphs. For the remaining 2,122 graphs, we obtained convergence to an excited state, mostly the first excited state, which explains the near-perfect performance in terms of the C/C_{max} metric. By switching on appropriately chosen pairs of edges, our modified linear QITE algorithm led to convergence to the ground state in all remaining 2,122 eight-vertex graphs. A pair of ITD edges also sufficed for ten-vertex graphs that we considered. Out of a randomly chosen sample of 200 graphs, 134 converged to the ground state with our algorithm using constant weights. The remaining 76 ten-vertex graphs also converged to the ground state after excising and gradually switching on a pair of edges that were appropriately chosen in each case.

Even though a large number of pairs of edges leads to convergence to the ground state, there appears to be no way of determining them from the graph. However, going through all possible combinations only adds a polynomial overhead ($O(|V|^2)$) to the calculation. It would be interesting to determine how the number of edges that need to be assigned weights that vary with imaginary time changes as larger graphs are analyzed. Our results indicate that
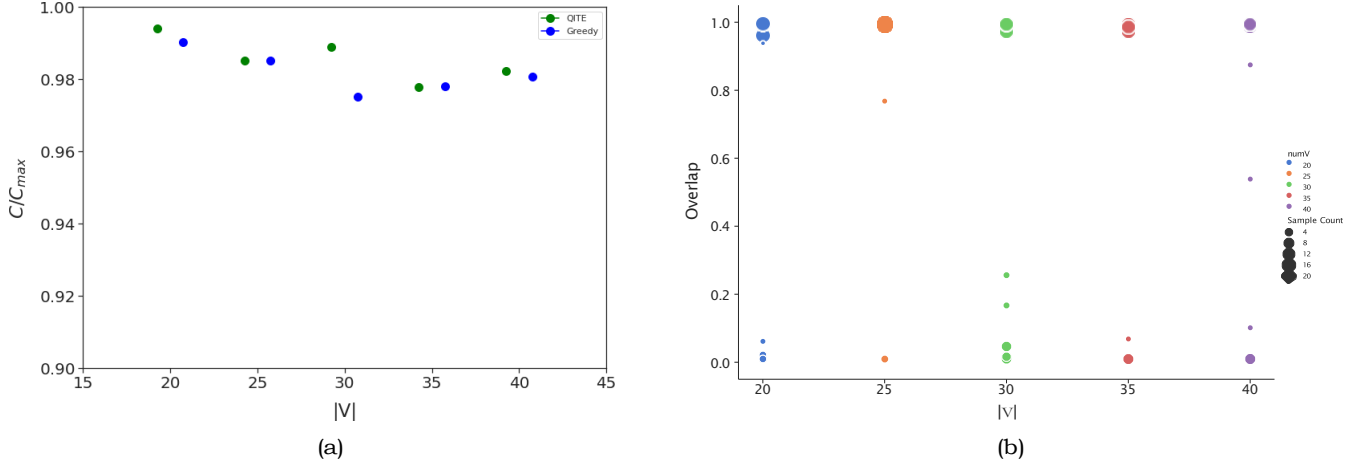
FIG. 9. (a) Average C/C_{max} comparison between QITE and a classical greedy algorithm. (b) Overlap with ground state for a random sample of graphs with number of vertices $|V|$ = {20, 25, 30, 35, 40}.

our linear QITE method offers an efficient solution to the MaxCut problem with complexity of the algorithm growing polynomially with the number of vertices $|V|$ of the graph.

The performance of our linear QITE algorithm remains robust on larger graphs. We applied the modified linear QITE algorithm with ITD edges to over 1,000 randomly chosen graphs with up to 50 vertices. The results are summarized in Figure 7(a). The blue line shows the performance of five steps of linear QITE whereas the green line shows the performance of the modified algorithm with two ITD edges showing significant performance improvement. The lowest C/C_{max} was found to be above 93%. This is above the performance of the Goemans-Williamson algorithm [8], which is the best known classical algorithm, at 88% approximation ratio for MaxCut.

Accumulated results for the graphs we analyzed with between 25 and 50 vertices are plotted in Figure 8 (blue line). It is important to note that the number of QITE steps needed to reach C/C_{max} above 93% is uniform, varying between 9 and 11, and does not grow with the number of vertices of the graphs. A performance comparison after applying s = 5 QITE steps to the worst performing graphs with the modified QITE method employing two ITD edges is shown in Figure 7(b).

All the graphs we analyzed above have been randomly chosen with edge probability between 9% and 99%. Next, we focus on less dense graph with edge probability randomly chosen between 3.5% and 4.5% per vertex which produces four edges per vertex on average. Figure 9(a) shows a comparison between QITE and a classical greedy algorithm[7]. Each green data point represents the average C/C_{max} over 25 different graphs calculated using QITE on randomly chosen graphs with the same number of vertices $|V|$ for $|V| \in$ {20, 25, 30, 35, 40}. We applied the modified QITE algorithm with ITD edges making 100 random selections of pairs of such edges from a total of $O(|V|^2)$ pairs and choosing the best result. The blue data points represent average C/C_{max} values of the same graphs obtained with a greedy algorithm. As we can see, the QITE performance is comparable to the performance of the classical greedy algorithm. Unlike the deterministic greedy algorithm, QITE is a probabilistic algorithm that yields a superposition state that we can take advantage of. QITE may converge to a superposition state that has a finite overlap with the ground state. In this case, one can obtain C_{max} even when the average C/C_{max} is less than 100%. Figure 9(b) shows the overlap with the ground state for the same graphs. Only four to seven among 25 graphs of a given number of vertices has zero overlap with the ground state. The rest of the graphs have non-vanishing overlap with most between 90% and 100% percent.

IV.   CONCLUSION

The ability of quantum algorithms to outperform their classical counterparts is primarily due to their ability to to tap the resource of quantum entanglement. In the case of combinatorial optimization, this is seen in QAOA [9] which introduces entanglement to solve a problem, such as MaxCut, in which both the initial state and desired final state are separable. However, despite considerable effort, quantum advantage is yet to be proved or demonstrated experimentally. QITE offers a different approach to combinatorial optimization by effectively cooling the system down

to its ground state and obtaining its minimum energy that corresponds to the optimal solution of the corresponding combinatorial optimization problem [39]. In general, QITE also introduces entanglement, but quantum advantage is yet to manifest.

In an effort to investigate the impact of entanglement on combinatorial optimization problems, we applied a version of QITE to the MaxCut problem that used a linear *Ansatz* for unitary updates and a separable initial state. Thus, we introduced no entanglement in the quantum algorithm which could be efficiently simulated by a classical computer. Remarkably, even though the linear updates introduced approximations at each step, for all graphs we analyzed our linear QITE algorithm succeeded in converging to the ground state, thus resulting in a performance exceeding 93% in terms of the metric $C/C_{\max}$. Importantly, the number of steps needed to reach that performance remained fairly uniform over the graphs we analyzed and did not grow with the number of vertices. Although further work on higher-order graphs is needed, our results indicate that our linear QITE method is efficient with the number of steps growing modestly with the number of vertices $|V|$ of the graph. In detail, we analyzed graphs with up to fifty vertices. After ten QITE steps using a Hamiltonian with constant weights, all graphs almost converged to an eigenstate of the Hamiltonian. A high percentage of them converged to the ground state. The remaining graphs converged to an excited state which, however, still led to very high performance in terms of the average $C/C_{\max}$ metric. The average $C/C_{\max}$ was found to be 89%. Furthermore, we were able to improve this performance and obtain convergence to the ground state, leading to average $C/C_{\max} \approx 97\%$ and worst performance of 93%, by considering an imaginary-time-dependent Hamiltonian resulting from excising a pair of edges appropriately chosen and switching them back on gradually within a few QITE steps. For each graph, we found several pairs of edges that led to the ground state. However, there appears to be no guidance on how to choose these edges in a given graph. Nevertheless, checking all possible pairs of vertices only introduces a polynomial overhead ($O(|V|^2)$) in the calculation.

To observe quantum advantage in the solution of the MaxCut problem, it appears to be necessary to consider graphs that are much larger than fifty-vertex graphs. This may take us outside the realm of NISQ devices as the depth of the quantum circuits will introduce a prohibitive amount of quantum errors. On the other hand, our work can be extended to larger graphs on which we can perform numerical calculations and investigate how complexity depends on the number of vertices and the role of entanglement. Entanglement can be introduced by adding higher-order terms to the unitary updates at each QITE step. It would be interesting to study what type of graphs with a large number of vertices can be accessed with NISQ devices at performance levels that exceed other quantum algorithms. Work in this direction is in progress.

[1] Frank Arute, Kunal Arya, Ryan Babbush, Dave Bacon, Joseph C Bardin, Rami Barends, Rupak Biswas, Sergio Boixo, Fernando GSL Brandao, David A Buell, et al. Quantum supremacy using a programmable superconducting processor. *Nature*, 574(7779):505–510, 2019.
[2] Han-Sen Zhong, Hui Wang, Yu-Hao Deng, Ming-Cheng Chen, Li-Chao Peng, Yi-Han Luo, Jian Qin, Dian Wu, Xing Ding, Yi Hu, Peng Hu, Xiao-Yan Yang, Wei-Jun Zhang, Hao Li, Yuxuan Li, Xiao Jiang, Lin Gan, Guangwen Yang, Lixing You, Zhen Wang, Li Li, Nai-Le Liu, Chao-Yang Lu, and Jian-Wei Pan. Quantum computational advantage using photons. *Science*, 2020.
[3] Paola Festa, Panos M Pardalos, Mauricio GC Resende, and Celso C Ribeiro. Randomized heuristics for the MAX-CUT problem. *Optimization methods and software*, 17(6):1033–1058, 2002.
[4] H. Schr¨oder, A.E. May, I. Vrt’o, and O. Sy´kora. Approximation algorithms for the vertex bipartization problem. In Franti˘sek Pl´a˘sil and Keith G. Jeffery, editors, *SOFSEM'97: Theory and Practice of Informatics*, pages 547–554, Berlin, Heidelberg, 1997. Springer Berlin Heidelberg.

[5] Sera Kahruman, Elif Kolotoglu, Sergiy Butenko, and I. Hicks. On greedy construction heuristics for the max-cut problem. *Int. J. of Computational Science and Engineering*, 1, 04 2007.

[6] Claire Mathieu and Warren Schudy. Yet another algorithm for dense max cut: Go greedy. In *Proceedings of the Nineteenth Annual ACM-SIAM Symposium on Discrete Algorithms*, SODA '08, page 176–182, USA, 2008. Society for Industrial and Applied Mathematics.

[7] Yatao Bian, Alexey Gronskiy, and Joachim M. Buhmann. Greedy maxcut algorithms and their information content. In *2015 IEEE Information Theory Workshop (ITW)*, pages 1–5, 2015.

[8] Michel X Goemans and David P Williamson. . 879-approximation algorithms for max cut and max 2sat. In *Proceedings of the twenty-sixth annual ACM symposium on Theory of computing*, pages 422–431, 1994.

[9] Edward Farhi, Jeffrey Goldstone, and Sam Gutmann. A quantum approximate optimization algorithm. *arXiv preprint arXiv:1411.4028*, 2014.

[10] Zhihui Wang, Stuart Hadfield, Zhang Jiang, and Eleanor G Rieffel. Quantum approximate optimization algorithm for maxcut: A fermionic view. *Physical Review A*, 97(2):022304, 2018.

[11] Stuart Hadfield. Quantum algorithms for scientific computing and approximate optimization. *arXiv preprint arXiv:1805.03265*, 2018.

[12] Leo Zhou, Sheng-Tao Wang, Soonwon Choi, Hannes Pichler, and Mikhail D. Lukin. Quantum approximate optimization algorithm: Performance, mechanism, and implementation on near-term devices. *Phys. Rev. X*, 10:021067, 2020.

[13] G G. Guerreschi and A. Y. Matsuura. QAOA for Max-Cut requires hundreds of qubits for quantum speed-up. *Scientific Reports*, 9, 2019.

[14] Matija Medvidovi´c and Giuseppe Carleo. Classical variational simulation of the quantum approximate optimization algorithm. *npj Quantum Information*, 7(1):1–7, 2021.

[15] Fernando G. S. L. Brandao, Michael Broughton, Edward Farhi, Sam Gutmann, and Hartmut Neven. For fixed control parameters the quantum approximate optimization algorithm's objective function value concentrates for typical instances. *arXiv preprint arXiv:1812.04170*, 2018.

[16] Jonathan Wurtz and Peter Love. Maxcut quantum approximate optimization algorithm performance guarantees for $p > 1$. *Phys. Rev. A*, 103:042612, Apr 2021.

[17] R. Shaydulin and Y. Alexeev. Evaluating quantum approximate optimization algorithm: A case study. In *2019 Tenth International Green and Sustainable Computing Conference (IGSC)*, pages 1–6, 2019.

[18] Gavin E Crooks. Performance of the quantum approximate optimization algorithm on the maximum cut problem. *arXiv preprint arXiv:1811.08419*, 2018.

[19] Ruslan Shaydulin, Stuart Hadfield, Tad Hogg, and Ilya Safro. Classical symmetries and the quantum approximate optimization algorithm. *Quantum Information Processing*, 20(11):359, October 2021.

[20] Rebekah Herrman, James Ostrowski, Travis S Humble, and George Siopsis. Lower bounds on circuit depth of the quantum approximate optimization algorithm. *Quantum Information Processing*, 20(2):1–17, 2021.

[21] V. Akshay, H. Philathong, M. E. S. Morales, and J. D. Biamonte. Reachability deficits in quantum approximate optimization. *Phys. Rev. Lett.*, 124:090504, 2020.

[22] Mario Szegedy. What do QAOA energies reveal about graphs? *arXiv preprint arXiv:1912.12277v2*, 2020.

[23] Guido Pagano, Aniruddha Bapat, Patrick Becker, Katherine S. Collins, Arinjoy De, Paul W. Hess, Harvey B. Kaplan, Antonis Kyprianidis, Wen Lin Tan, Christopher Baldwin, Lucas T. Brady, Abhinav Deshpande, Fangli Liu, Stephen Jordan, Alexey V. Gorshkov, and Christopher Monroe. Quantum approximate optimization of the long-range Ising model with a trapped-ion quantum simulator. *Proceedings of the National Academy of Sciences*, 117(41):25396–25401, 2020.

[24] Zhihui Wang, Nicholas C Rubin, Jason M Dominy, and Eleanor G. Rieffel. *XY*-mixers: analytical and numerical results for the quantum alternating operator ansatz. *Physical Review A*, 101:012320, 2020.

[25] Linghua Zhu, Ho Lun Tang, Gearge S. Barron, Nicholas J. Mayhall, Edwin Barnes, and Sophia E. Economou. An adaptive quantum approximate optimization algorithm for solving combinatorial problems on a quantum computer. *arXiv preprint arXiv:2005.10258*, 2020.

[26] Zhang Jiang, Eleanor G. Rieffel, and Zhihui Wang. Near-optimal quantum circuit for Grover's unstructured search using a transverse field. *Physical Review A*, 95:062317, 2017.

[27] Andreas B¨artschi and Stephan Eidenbenz. Grover mixers for QAOA: Shifting complexity from mixer design to state preparation. *arXiv preprint arXiv:2006.00354v2*, 2020.

[28] Jeremy Cook, Stephan Eidenbenz, and Andreas B¨artschi. The quantum alternating operator ansatz on maximum k-vertex cover. *arXiv preprint arXiv:1910.13483v2*, 2020.

[29] Li Li, Minjie Fan, Marc Coram, Patrick Riley, and Stefan Leichenauer. Quantum optimization with a novel Gibbs objective function and ansatz architecture search. *Phys. Rev. Research*, 2, 2020.

[30] Reuben Tate, Majid Farhadi, Creston Herold, Greg Mohler, and Swati Gupta. Bridging classical and quantum with SDP initialized warm-starts for QAOA. *arXiv preprint arXiv:2010.14021*, 2020.

[31] Rebekah Herrman, Phillip C Lotshaw, James Ostrowski, Travis S Humble, and George Siopsis. Multi-angle quantum approximate optimization algorithm. *Scientific Reports*, 12(1):6781, April 2022.

[32] M. B. Hastings. Classical and quantum bounded depth approximation algorithms. *arXiv preprint arXiv:1905.07047*, 2019.

[33] Aniruddha Bapat and Stephen P. Jordan. Approximate optimization of the maxcut problem with a local spin algorithm. *Phys. Rev. A*, 103:052413, May 2021.

[34] Kunal Marwaha. Local classical MAX-CUT algorithm outperforms $p = 2$ QAOA on high-girth regular graphs. *Quantum*, 5:437, April 2021.

[35] Kunal Marwaha and Stuart Hadfield. Bounds on approximating Max kXOR with quantum and classical local algorithms.

Quantum, 6:757, jul 2022.

[36] Sam McArdle, Tyson Jones, Suguru Endo, Ying Li, Simon C. Benjamin, and Xiao Yuan. Variational ansatz-based quantum simulation of imaginary time evolution. *npj Quantum Information*, 5(1):75, Sep 2019.

[37] Matthew JS Beach, Roger G Melko, Tarun Grover, and Timothy H Hsieh. Making trotters sprint: A variational imaginary time ansatz for quantum many-body systems. *Physical Review B*, 100(9):094434, 2019.

[38] Peter J Love. Cooling with imaginary time. *Nature Physics*, 16(2):130–131, 2020.

[39] Mario Motta, Chong Sun, Adrian TK Tan, Matthew J O'Rourke, Erika Ye, Austin J Minnich, Fernando GSL Brandao, and Garnet Kin-Lic Chan. Determining eigenstates and thermal states on a quantum computer using quantum imaginary time evolution. *Nature Physics*, 16(2):205–210, 2020.

[40] Niladri Gomes, Feng Zhang, Noah F Berthusen, Cai-Zhuang Wang, Kai-Ming Ho, Peter P Orth, and Yongxin Yao. Efficient step-merged quantum imaginary time evolution algorithm for quantum chemistry. *Journal of Chemical Theory and Computation*, 16(10):6256–6266, 2020.

[41] Kübra Yeter-Aydeniz, Raphael C Pooser, and George Siopsis. Practical quantum computation of chemical and nuclear energy levels using quantum imaginary time evolution and lanczos algorithms. *npj Quantum Information*, 6(1):1–8, 2020.

[42] Kübra Yeter-Aydeniz, Bryan T Gard, Jacek Jakowski, Swarnadeep Majumder, George S Barron, George Siopsis, Travis S Humble, and Raphael C Pooser. Benchmarking quantum chemistry computations with variational, imaginary time evolution, and krylov space solver algorithms. *Advanced Quantum Technologies*, page 2100012, 2021.

[43] Stefano Barison, Davide Emilio Galli, and Mario Motta. Quantum simulations of molecular systems with intrinsic atomic orbitals. *arXiv e-prints*, page arXiv:2011.08137, November 2020.

[44] Hirsh Kamakari, Shi-Ning Sun, Mario Motta, and Austin J Minnich. Digital quantum simulation of open quantum systems using quantum imaginary time evolution. *arXiv preprint arXiv:2104.07823*, 2021.

[45] Jean-Loup Ville, Alexis Morvan, Akel Hashim, Ravi K Naik, Bradley Mitchell, John-Mark Kreikebaum, Kevin P O'Brien, Joel J Wallman, Ian Hincks, Joseph Emerson, et al. Leveraging randomized compiling for the qite algorithm. *arXiv preprint arXiv:2104.08785*, 2021.

[46] Chenfeng Cao, Zheng An, Shi-Yao Hou, D. L. Zhou, and Bei Zeng. Quantum imaginary time evolution steered by reinforcement learning, 2021.

[47] Hirofumi Nishi, Taichi Kosugi, and Yu-ichiro Matsushita. Implementation of quantum imaginary-time evolution method on nisq devices by introducing nonlocal approximation. *npj Quantum Information*, 7(1):85, Jun 2021.

[48] Sheng-Hsuan Lin, Rohit Dilip, Andrew G. Green, Adam Smith, and Frank Pollmann. Real- and imaginary-time evolution with compressed quantum circuits. *PRX Quantum*, 2:010342, Mar 2021.

[49] Stuart Hadfield, Zhihui Wang, Bryan O'Gorman, Eleanor G Rieffel, Davide Venturelli, and Rupak Biswas. From the quantum approximate optimization algorithm to a quantum alternating operator ansatz. *Algorithms*, 12(2):34, 2019.